6202 *Macromolecules* **2010**, *43*, 6202–6212
DOI: 10.1021/ma902823k

Macromolecules
ARTICLE

# Application of the Slip-Link Model to Bidisperse Systems

**Renat N. Khaliullin* and Jay D. Schieber***

*Center for Molecular Study of Condensed Soft Matter, Department of Chemical and Biological Engineering, and Department of Biological, Chemical, and Physical Sciences, Illinois Institute of Technology, 3440 South Dearborn Street, Chicago, Illinois*

*Received December 22, 2009; Revised Manuscript Received May 27, 2010*

ABSTRACT: Although the LVE predictions of monodisperse systems by the discrete slip-link model (DSM) are at least as good as those made by tube models, there are significant differences in contributions to relaxation from polymer chain dynamics and environment dynamics (Khaliullin et al. *Macromolecules* **2009**, *42*, 7504−7517). This observation suggests that tube models and DSM might yield different predictions for the observable relaxation modulus of bidisperse blends. Here we compare DSM to experimental data as well as the Park and Larson tube model (Park et al. *Macromolecules* **2004**, *37*, 597−604) and the des Cloizeaux tube model with modified double reptation (van Ruymbeke et al. *Macromolecules* **2002**, *35*, 2689−2699). Our self-consistent implementation of constraint dynamics avoids factorization assumptions, or tube dilation processes, so no new parameter, such as the Struglinski-Graessley parameter, is necessary. All three models compare very well with experiments. We then use the DSM to analyze the molecular probe rheology experiments of Liu et al. (Liu et al. *Macromolecules* **2006**, *39*, 7415−7424). By examining the dynamic modulus of blends of very long and short entangled chains, those authors concluded that constraint release plays a significant role in molecular weight scaling of the longest relaxation time. Here we show that their conclusion is incorrect because their analysis neglects constraint dynamics of the long chains. Moreover, we show that a correct analysis can be used to distinguish between tube and slip-link models. Namely, probe rheology can be used to estimate a sum of relaxation from sliding dynamics and constraint dynamics. Because the dynamic modulus of monodisperse systems measures a product of these two processes, the combination of the two experiments can be used to distinguish between sliding and constraint dynamics. Only DSM can describe both experiments.

## Introduction

Polydispersity is present in all polymers and significantly affects polymer melt linear viscoelastic (LVE) measurements,[2,3,7,8,10−12] which makes LVE a useful tool for polydispersity characterization. Unfortunately, current atomistic simulations are able to resolve relaxation times up to a few hundred nanoseconds only, so are incapable of resolving time scales necessary for LVE prediction.[13] Therefore, to make LVE predictions, it is necessary to develop a coarse-grained model or, even more favorable, a coarse-grained mean-field model, which utilizes a level of description less detailed than molecular simulations.

There are many mean-field models that predict LVE for monodisperse systems very well.[5,10,14−18] These models assume that the main determinant of stress relaxation in polymer melts is entanglement dynamics. Entanglements are topological constraints that account for entropic changes in polymer conformations related to chain uncrossability. Due to Brownian forces and free-energy differences, a polymer chain slides through the entanglements relaxing its stress. At the same time, it has been shown that LVE for a blend is not a superposition of LVE for its monodisperse components,[10] indicating that polymer relaxation cannot be approximated by a mean-field chain in the presence of fixed obstacles. Rather, chain−chain interactions are essential in polymer dynamics.

Chain−chain interactions in mean-field tube models are implemented by a constraint release (CR) process, which removes stress from the middle of the chain. There are several mathematical frameworks that describe CR: "double reptation" (DR),[15] Rouse motion,[10,14,19] and tube dilation.[1,5,18,20] It has been shown by Likhtman and McLeish that for monodisperse polymers CR modeled as a Rouse motion predicts LVE very well.[14] The Rouse motions of the entanglements were implemented by representing the tube as a 3D bead−spring chain, where each bead has a fixed mobility that is chosen consistently with sliding dynamics (SD) of the polymer chains surrounding the tube.

In a recent work we compared the discrete slip-link model (DSM) with monodisperse LVE data.[4] We showed that the new self-consistent implementation of the chain−chain interactions in DSM as constraint dynamics (CD) agrees with data well. Note that the CD process destroys and creates entanglements in the middle of the chain, in contrast to CR, which does not affect the number of entanglements per chain. We also compared the DSM monodisperse LVE predictions with those by the Likhtman and McLeish model.[14] The differences between the model predictions were within the experimental uncertainty. Because the slip-link model is more detailed, physical ideas, such as CLF, reptation, and so on, arise naturally from the model rather than being added by hand, as is typical in tube models. As a result of the higher level of description, we could examine several assumptions made by Likhtman and McLeish. From comparison of these models, we determined, in agreement with tube theory, that (*i*) the total relaxation modulus for the monodisperse system, $G(t)$, is proportional to a product of the relaxation modulus from chain sliding dynamics (SD), $G^{SD}(t)$, and the relaxation modulus from CD, $G^{CD}(t)$, (*ii*) the probability of primitive-path survival can be separated into contour-length fluctuations (CLF) and reptation,

*To whom correspondence should be addressed. E-mail: rkhaliul@iit.edu (R.N.K.); schieber@iit.edu (J.D.S.).

 Published on Web 06/22/2010 

and (*iii*) CD does not significantly affect zero-shear-rate viscosity scaling and the SD terminal time in monodisperse systems. On the other hand, several other tube theory assumptions disagree with the DSM. Namely, $G^{SD}(t)$ can not be approximated by a fraction of survived primitive-path times the plateau modulus, $G_N^0$, plus longitudinal modes; and chain−chain interactions are not well approximated by a 3D Rouse motion of permanent entanglements. These assumptions introduce errors when applied to the DSM. Those errors cancel each other when CR and SD relaxation moduli are multiplied. As a result, the LVE predictions of the two models are nearly indistinguishable when compared with monodisperse LVE experimental data. However, we expect these differences to result in different predictions of LVE for polydisperse mixtures, which motivates our work here.

Unfortunately, there is no self-consistent tube model for polydisperse systems, as detailed as that by Likhtman and McLeish for monodisperse systems.[14] The most-studied tube model prediction for polydisperse polymer mixtures is double reptation (DR). DR assumes that the polymer relaxation modulus, $G(t)$, can be factorized into the product of two independent relaxation moduli $G^{SD}(t)$ and $G^{CR}(t)$. It also assumes that for monodisperse polymers $G^{CR}(t) \cong G^{SD}(t)$.[15] However, van Ruymbeke et al. showed that better agreement with experiments is achieved if one assumes that $G^{CR}(t) \propto (G^{SD}(t))^{1.25}$ for tube models so that the terminal time of the blend would decrease compared to the long-chain monodisperse system. The higher exponent in the DR model is hypothesized to arise from the existence of entanglements that involve more than 2 chains.[3]

Another explanation for the decrease of the blend terminal time is an influence of CR on SD. Such an influence is neglected by assuming independence of the relaxation moduli, so the influence is added ad hoc. In addition, Struglinski and Graessley experimentally showed that for blends with sufficiently large difference between long and short chain molecular weights the longest relaxation time of the blend is significantly smaller than the longest relaxation of its high-molecular-weight monodisperse component.[21] That decrease was not captured by erstwhile existing tube models, so it was accounted for by adding new physics to the model, such as tube dilation. However, such a process can not be applied to the blends of similar molecular weight, because it reduces the longest relaxation time too much. As a result, Struglinski and Graessley introduced a parameter that determines if tube dilation takes place or not in tube models. The critical value of the Struglinski-Graessley parameter SG: $= M_e^2 M_L / M_S^3$ was set to 1. Later Park and Larson developed a new tube model that mimics CR as a combination of Rouse motion and concentration-dependent modulus. They find that the critical value of the SG parameter for their model is 0.064. We show below that our DSM requires no such considerations as the SG parameter, but can still describe the decrease in the blend terminal time.

More recently Liu et al. looked at bidisperse blends of widely separated molecular weights in order to minimize the contribution from chain−chain interactions to the relaxation of a small fraction of probe chains in a matrix of long chains.[22]They assumed that relaxation of the matrix of long chains is negligible on the time scale of relaxation of probe chains. As a result, they attempted to extract relaxation of the probe chains in a matrix of nearly fixed entanglements. Based on their experimental results, they concluded that existing tube models overestimate polymer relaxation contribution from the CLF compared to the reptation process. In addition, they concluded that presence of constraint dynamics affects zero-shear-rate viscosity scaling with molecular weight. In our previous paper we compared Liu et al. experimental results with the discrete slip-link model prediction for chains in a fixed environment.[4] We found a disagreement with their conclusions. We suspected that the source of the disagreement is relaxation of the matrix due to CD of the probe chains on the long chains, which is on the same time scale as relaxation of the probe chains. In this work we will also examine the contribution to CD on the long chains of the Liu et al. experiments. The results confirm our suspicions.

Here we apply the DSM to bidisperse systems without any modifications. The model can also be applied to blends of higher dispersity, but we believe that systems with two distinct molecular weights provide a more severe test. We compare our LVE predictions to experimental results and to predictions by the des Cloizeaux time-dependent diffusion tube model combined with modified double reptation (TDD-MDR), as suggested by van Ruymbeke et al.,[3] and with the Park and Larson (PL) tube model.[5] We show that the DSM with binary entanglements agrees with data at least as well as the TDD-MDR model with its ad hoc exponent of 2.25. We show that fundamental implementation of chain−chain interactions as CD predicts well bidisperse blends of various molecular-weight separations including systems with SG < 0.064, 0.064 < SG < 1 and 1 < SG. It does not require ad hoc parameters or any additional physics such as tube dilation combined with SG criteria. In addition, we show how to generalize the DSM to entanglements that contain an arbitrary number of chains and examine LVE sensitivity to the assumption of binary entanglements.

## Discrete Slip-Link Model

The discrete slip-link model (DSM) was introduced in ref 17 and significantly evolved in a recent work.[4] Details are given there. Here we describe the model briefly and show how to apply it to polydisperse systems.

The chain is approximated by a random walk. The entanglements are randomly distributed along the chain with uniform probability $1/(1+\beta)$, defining the primitive-path of the chain, where $\beta$ is a model parameter that is defined below. It is assumed that relaxation of an entangled strand is much faster then the chain relaxation, so the chain may be coarse-grained to a primitive-path. The model is described by the following variables: the number of strands, $Z$, in a chain; the number of Kuhn steps, $N_i$, in the $i^{th}$ strand; the vector, $\boldsymbol{Q}_i$, connecting entanglements $i-1$ and $i$; and the characteristic lifetime, $\tau_i^{CD}$, of the $i^{th}$ entanglement related to constraint dynamics (CD). The equilibrium probability density, $p_{eq,\gamma}(\Omega)$, of conformations of a type $\gamma$ chain, which denotes chain length, is given by the modified Maxwell−Boltzmann relationship

$$p_{eq,\gamma}(\Omega) = \frac{\delta(N_{K,\gamma}, \sum_{i=1}^{Z} N_i)}{J\beta^{Z-1}} \exp\left[-\frac{F(\Omega)}{k_B T}\right] \prod_{i=1}^{Z-1} p^{CD}(\tau_i^{CD}) \quad (1)$$

where $J = (1+1/\beta)^{N_K} - 1$ is the normalization constant, $\delta(i,j)$ is the Kronecker delta function, $N_{K,\gamma}$ is the total number of Kuhn steps in a chain of type $\gamma$, $F(\Omega)$ is the free energy of achain with conformation $\Omega$, $T$ is temperature, $p^{CD}(\tau^{CD})$ is the probability density of entanglement lifetimes, $k_B$ is the Boltzmann constant, and $\beta$ is a parameter that depends on entanglement density and approximately equal to $N_e - 1$ for long chains, where $N_e \equiv \langle N_i \rangle$ is the average number of Kuhn steps in a strand.[4]

Here, the free energy of an entangled strand is approximated by the Gaussian free energy[17]

$$\frac{F_s(\boldsymbol{Q}, N)}{k_B T} = \frac{3Q^2}{2Na_K^2} + \frac{3}{2}\ln\left[\frac{2\pi N}{3a_K^2}\right] \quad (2)$$

The approximation is valid for flexible polymer chains that are not stretched greater than about 1/3 of their contour length. The

free energy of the dangling ends is found to be zero, so the free energy of the entire chain is

$$F(\Omega) = \sum_{i=2}^{Z-1} F_s(\boldsymbol{Q}_i, N_i) \tag{3}$$

In DSM, $N_i$ is treated as an integer number, so conformation changes due to Brownian forces are described by a jump process from one conformation to another. The evolution equation at equilibrium becomes

$$\frac{\partial p_{eq,\gamma}(\Omega, t|\Omega_0, t_0)}{\partial t} = \int [W(\Omega|\Omega') p_{eq,\gamma}(\Omega', t|\Omega_0, t_0) - W(\Omega'|\Omega) p_{eq,\gamma}(\Omega, t|\Omega_0, t_0)] d\Omega' \tag{4}$$

where $W(\Omega'|\Omega)$ is a transition rate probability of a jump from conformation $\Omega$ to $\Omega'$ in unit time. $\tau_K$ is a characteristic time required to shift one Kuhn step through an entanglement, which depends on the polymer chemistry and temperature, but not the polymer architecture nor molecular weight. Note that jumps to conformation $\Omega$ are allowed only from a neighboring conformation $\Omega'$, so $W(\Omega|\Omega')$ can be split into five processes

$$W = (\sum_{i=1}^{Z-1} W_{sh}^i) + W_d^{SD} + W_c^{SD} + W_d^{CD} + W_c^{CD} \tag{5}$$

where $W_{sh}^i$ is a transition probability per time to shift a Kuhn step through entanglement $i$, $W_d^{SD}$ and $W_c^{SD}$ are related to probabilities to destroy and create an entanglement on the ends of the chain by SD, and $W_d^{CD}$ and $W_c^{CD}$ are transition probabilities per time to destroy and create an entanglement in the middle of the chain by CD. Complete expressions for the transition probabilities are reported in ref 4.

In DSM an entanglement is formed by at least two chains, so if one chain abandons an entanglement then it should be destroyed for the other chain(s). The simplest realization of such CD would be to couple several chains in the ensemble as was done by Doi and Takimoto.[23] However, such an implementation loses some advantages of a mean-field theory. To develop a self-consistent realization with independent chains in the ensemble we add a characteristic lifetime, $\tau^{CD}$, to each entanglement. The distribution of the lifetimes, $p^{CD}(\tau^{CD})$, will affect the rate of destruction of the entanglements by CD, which should be self-consistent with the rate of destruction by SD.[4] $p^{CD}(\tau^{CD})$ is defined by chain−chain interactions, so it depends on polydispersity and complexity of entanglements. We show how to calculate $p^{CD}(\tau^{CD})$ for a polydisperse blend with any average number of chains, $\alpha$, entangled with the probe chain. We assume that any given entanglement consists of an integer number of chains, but on average the number can be noninteger. If $\alpha$ is a noninteger, the simplest implementation is to allow only entanglements with the two integer numbers of chains closest to $\alpha$. Although, more realistic might be to use a Poisson distribution; we are interested here in sensitivity effects of entanglement complexity. $p^{CD}(\tau^{CD})$ is found in a self-consistent way from chain SD using the following equation

$$p^{CD}(\tau^{CD}) = (\mathrm{int}(\alpha) - \alpha) \underbrace{\int_0^\infty \cdots \int_0^\infty}_{\mathrm{int}(\alpha)-1} \delta\left(\tau^{CD} - 1 \Big/ \sum_{i=1}^{\mathrm{int}(\alpha)-1} \frac{1}{\tau_i}\right) \prod_{i=1}^{\mathrm{int}(\alpha)-1} p^{SD}(\tau_i) d\tau_i + (\alpha - \mathrm{int}(\alpha) + 1) \underbrace{\int_0^\infty \cdots \int_0^\infty}_{\mathrm{int}(\alpha)} \delta\left(\tau^{CD} - 1 \Big/ \sum_{i=1}^{\mathrm{int}(\alpha)} \frac{1}{\tau_i}\right) \prod_{i=1}^{\mathrm{int}(\alpha)} p^{SD}(\tau_i) d\tau_i, \tag{6}$$

where int($\alpha$) is the smallest integer value that is equal to or greater than $\alpha$. $p^{SD}(\tau)$ is obtained from the fraction of survived entanglements, $f^{SD}(t)$, that are being destroyed by SD only

$$f^{SD}(t) = \int_0^\infty p^{SD}(\tau) \exp\left(-\frac{t}{\tau}\right) d\tau \tag{7}$$

For binary entanglements ($\alpha = 1$), eq 6 becomes equivalent to that used in refs 4,10, and 14.

For a polydisperse blend of $n_m$ components with volume fractions $w_\gamma$, $f^{SD}(t)$ is split into a fraction of survived entanglements of the individual components $f_\gamma^{SD}(t)$ as follows

$$f^{SD}(t) = \sum_{\gamma=1}^{n_m} w_\gamma f_\gamma^{SD}(t) \tag{8}$$

Note that, for the blends considered in this paper, volume and weight fractions are assumed to be the same, so we choose to use weight fraction. However, in a more complicated blend, volume fraction would be more appropriate.

We assume that entanglement characteristic lifetimes are all independent, ignoring the fact that two chains once entangled have a higher chance to entangle again, so $p^{CD}(\tau^{CD})$ is not affected by neighboring values of $\tau^{CD}$. Assuming binary interactions and using eqs 6 and 8, $p^{CD}(\tau^{CD})$ is constructed from lifetime distributions of its monodisperse components

$$p^{CD}(\tau^{CD}) = \sum_{\gamma=1}^{n_m} w_\gamma p_\gamma^{CD}(\tau^{CD}) \tag{9}$$

where $p_\gamma^{CD}(\tau^{CD})$ is the entanglement characteristic lifetime distribution for the $\gamma^{th}$ component. Details on how $p_\gamma^{CD}(\tau^{CD})$ is estimated for a monodisperse component are given in ref 4 and the result has the following form

$$p_\gamma^{CD}(\tau) = \frac{(1-g_\gamma)\alpha_\gamma}{(\tau_\gamma^{max})^{\alpha_\gamma} - (\tau_\gamma^0)^{\alpha_\gamma}} \tau^{\alpha_\gamma - 1} H(\tau - \tau_\gamma^0) H(\tau_\gamma^{max} - \tau) - g_\gamma \delta(\tau_\gamma^d - \tau) \tag{10}$$

where $g_\gamma$, $\alpha_\gamma$, $\tau_\gamma^0$, $\tau_\gamma^{max}$, and $\tau_\gamma^d$ are parameters determined self-consistently by $\tau_K$, $N_{K,\gamma}$, and $\beta$. $H(x)$ is the Heaviside step function. The first term is a result of CLF and the second term is related to reptation.[4]

After calculating $p^{CD}(\tau^{CD})$ and using it in eq 1, we predict the relaxation modulus of the blend, $G(t)$ by using the Green-Kubo expression

$$G(t) = \frac{V}{k_B T} \langle \tau_{xy}(0) \tau_{xy}(t) \rangle_{eq} \tag{11}$$

where $\langle \cdots \rangle_{eq}$ is an ensemble average, $\tau_{xy}(t)$ is any off-diagonal stress tensor component and $V$ is the system volume. Note, that the DSM is a mean-field model, so the stress tensor of the system is a sum of the stresses of its individual chains per unit volume

$$\tau = \frac{1}{V} \sum_{j=1}^{N_c} \tau_j^c \tag{12}$$

where $N_c$ is the total number of chains. The chain stress tensor is found from thermodynamics[17,24]

$$\tau_j^c(t) = -\sum_{i=2}^{Z_j - 1} \boldsymbol{Q}_{i,j} \left(\frac{\partial F(\Omega)}{\partial \boldsymbol{Q}_{i,j}}\right)_{T, \{N_{i,j}\}, \boldsymbol{Q}_{k \neq i,j}} \tag{13}$$

Using eqs 11−13, we calculate the relaxation modulus of the system to be

$$G(t) = \sum_{\gamma=1}^{n_m} w_\gamma G_\gamma(t) \tag{14}$$

where $G_\gamma(t)$ is the relaxation modulus of the $\gamma^{\text{th}}$ component in the system.

To obtain the dynamic modulus, $G^*(\omega)$, we fit a relaxation spectrum, $h_\gamma(\tau)$, to $G_\gamma(t)$

$$G_\gamma(t) = G^0_{\text{N},\gamma}\int_0^\infty \frac{h_\gamma(\tau)}{\tau}\exp\left(-\frac{t}{\tau}\right)\mathrm{d}\tau \tag{15}$$

We find that $h_\gamma(\tau)$, represented by a BSW spectrum,[25] describes model predictions very well

$$h_\gamma(\tau) = \sum_{k=1}^{l_\gamma}\frac{g_{k,\gamma}\alpha_{k,\gamma}\tau^{\alpha_{k,\gamma}}H(\tau^{\max}_{k,\gamma}-\tau)H(\tau-\tau^0_{k,\gamma})}{(\tau^{\max}_{k,\gamma})^{\alpha_{k,\gamma}}-(\tau^0_{k,\gamma})^{\alpha_{k,\gamma}}} \tag{16}$$

where $g_{k,\gamma}$, $\alpha_{k,\gamma}$, $\tau^0_{k,\gamma}$, $\tau^{\max}_{k,\gamma}$ are the fitting parameters and $l_\gamma$ is the number of fitting modes for the $\gamma$ component. We find that $l_\gamma = 1$ is enough for the low-molecular-weight component, and $l_\gamma = 2$ is for the high-molecular-weight component in bidisperse blends.

The dynamic moduli, $G^*_\gamma(\omega)$, are calculated analytically from the one-sided Fourier transform of eq 15 multiplied by $i\omega$. The expressions for $G'_\gamma(\omega)$ and $G''_\gamma(\omega)$ are

$$G'_\gamma(\omega) = G^0_{N,\gamma}\omega^2\sum_{i=1}^{m}\frac{\prod_{j=0}^{i-1}\tau_j^{\alpha_j-\alpha_{j+1}}}{\alpha_i+2}\left[{}_2F_1\left(1,\frac{\alpha_i+2}{2};\frac{\alpha_i+4}{2};-\omega^2\tau_i^2\right)\tau_i^{\alpha_i+2}-{}_2F_1\left(1,\frac{\alpha_i+2}{2};\frac{\alpha_i+4}{2};-\omega^2\tau_{i-1}^2\right)\tau_{i-1}^{\alpha_i+2}\right]\Bigg/\sum_{i=1}^{m}\frac{\prod_{j=0}^{i-1}\tau_j^{\alpha_j-\alpha_{j+1}}(\tau_i^{\alpha_i}-\tau_{i-1}^{\alpha_i})}{\alpha_i} \tag{17}$$

$$G''_\gamma(\omega) = G^0_{N,\gamma}\omega\sum_{i=1}^{m}\frac{\prod_{j=0}^{i-1}\tau_j^{\alpha_j-\alpha_{j+1}}}{\alpha_i+1}\left[{}_2F_1\left(1,\frac{\alpha_i+1}{2};\frac{\alpha_i+3}{2};-\omega^2\tau_i^2\right)\tau_i^{\alpha_i+1}-{}_2F_1\left(1,\frac{\alpha_i+1}{2};\frac{\alpha_i+3}{2};-\omega^2\tau_{i-1}^2\right)\tau_{i-1}^{\alpha_i+1}\right]\Bigg/\sum_{i=1}^{m}\frac{\prod_{j=0}^{i-1}\tau_j^{\alpha_j-\alpha_{j+1}}(\tau_i^{\alpha_i}-\tau_{i-1}^{\alpha_i})}{\alpha_i} \tag{18}$$

where ${}_2F_1(a, b, c, d)$ is the hypergeometric function. Using eqs 14, 17, and 18, we calculate the dynamic modulus of the polydisperse blend.

## Tube Models for Polydisperse Systems

The level of description of the DSM allows prediction of LVE from the terminal relaxation up to longitudinal modes. The tube models find that the parameter necessary to describe longitudinal modes can also predict high frequency modes (sometimes called Rouse modes), although Likhtman and McLeish reported some nonuniversality of polybutadiene.[14] In the DSM we do not specify relaxation processes separately, thus we can not make any conclusion about high frequency modes. As a result, here we compare DSM with tube models that include only physics (or parameters) that are necessary to describe the terminal time, primitive-path-length fluctuations, and longitudinal modes.

A successful tube model that predicts LVE of polydisperse systems is a TDD-MDR proposed by van Ruymbeke et al.[3] Although we are aware of a more recent tube model by van Ruymbeke et al.,[31] we will avoid comparison in this paper. The model is solved numerically, so it requires development of a mathematical code. On the other hand, the main objective of this work is to show that DSM with CD using only two adjustable parameters ($\beta$ and $\tau_K$) can predict bidisperse mixtures at least as well as other models that require more parameters. The latest van Ruymbeke model requires six parameters ($G^0_N$, $M_e$, $\tau_e$, $\tau_R$, $\alpha$, and SG) for bidisperse predictions, but gives similar agreement with experiments. However, $\alpha$ has a fixed value, which is equal to 1 in recent work,[31] and therefore is not an adjustable parameter. In addition, $M_e$ has a relationship with $G^0_N$, thus, the model actually has only four adjustable parameters. Of course, van Ruymbeke's model is much easier to calculate than DSM.

The TDD-MDR assumes that LVE of a polydisperse blend can be found from the relaxation moduli of its monodisperse components by using the mixing rule

$$G(t) = G^0_N\left[\int w(M)\left(\frac{G(M,t)}{G^0_N}\right)^{1/(\alpha+1)}\frac{\mathrm{d}M}{M}\right]^{\alpha+1} \tag{19}$$

where $M$ is polymer molecular weight, $w(M)$ is the weight fraction of the polymer, $G(M, t)$ is the relaxation modulus of the polymer, and $\alpha$ is a model parameter. For $\alpha$ equal to 1 the model predicts double reptation, however, 1.2 gives better agreement with polydisperse LVE data.

LVE predictions of the monodisperse components are obtained assuming that the relaxation modulus is factorized in the following way

$$\frac{G_{\text{TDD}}(t,M)}{G^0_N} = \frac{8}{\pi}\sum_{p\text{odd}}\frac{1}{p^2}\exp\left(-\frac{p^2t}{K_rM^3}\right)\exp\left[-\frac{p^2M^*}{M}g\left(\frac{t}{M^*K_rM^2}\right)\right] + \frac{M_e}{3M}\sum_{p=1}^{M/M_e}\exp\left(-\frac{p^2t}{K_RM^2}\right) \tag{20}$$

$$g(y)\simeq\sqrt{y}\sqrt{y+\sqrt{\pi y}+\pi}-y \tag{21}$$

where $K_r$, $K_R$, $M^*$, $M_e$, and $G^0_N$ are model parameters. The second term in eq 20 is the longitudinal modes[3] similar to that by the Likhtman and McLeish tube model.[14] The high frequency modes were removed from the model for fair comparison, although the longitudinal modes are kept. The parameter values for polystyrene are $M^* = 160$ kDa, $M_e = 18.5$ kDa, and $\alpha = 1.2$;[3] other parameters ($K_r$, $K_R$, and $G^0_N$) are treated as adjustable. Therefore, the TDD-MDR model has six parameters to predict polydisperse LVE.

Recently, another tube model was developed by Park and Larson that successfully predicts polydisperse LVE.[5,26] The model is similar to the Milner and McLeish tube model for branched systems.[27] We present here our own interpretation of the model based on equations given in their papers assuming $\alpha = 1$, as suggested.[5]

As shown in eq 15, the relaxation modulus is characterized by a relaxation spectrum $h(\tau)$. With only SD present, the relaxation

spectrum for $G^{SD}(t)$ is assumed by Park and Larson to split into two distinct processes with different characteristic time scales

$$h^{SD}(\tau) = h^{SD}_{CLF}(\tau) + h^{SD}_{rep}(\tau) \tag{22}$$

where $h^{SD}_{CLF}(\tau)$ represents the relaxation spectrum related to the contour-length fluctuation contribution to the relaxation modulus and $h^{SD}_{rep}(\tau)$ is the relaxation spectrum for the chain reptation contribution. Consistent with Rubinstein and Colby[10] and with Likhtman and McLeish,[14] these spectra are modeled by Park and Larson as

$$\begin{aligned} h^{SD}_{CLF} &:= \frac{1}{4}\left(\frac{256\tau}{9\pi^2 Z^4 \tau_e}\right)^{1/4}(1 - U(\tau - \tau_d)) \\ h^{SD}_{rep} &:= \frac{8}{\pi^2}\left[1 - \left(\frac{256\tau_d}{9\pi^2\tau_e Z^4}\right)^{1/4}\right]\sum_{p\text{odd}} \tau\delta(\tau - \tau_d/p^2) \end{aligned} \tag{23}$$

where $U(t)$ is the unit step function[28] and $\tau_d$ is the reptation time. The reptation time is defined as

$$\tau_d = 3Z^3\tau_e\left(1 - \frac{8\sqrt{\sqrt{3}\pi^{3/2}Z^2 + 4} - 16}{2\sqrt{3}\pi^{3/2}Z^2}\right)^2 \tag{24}$$

$Z = M/M_e$ is the number of strands in a chain, $M_e$ is the entanglement molecular weight, and $\tau_e$ is the model time scale.

When CR is added to the model, $G^{SD}$ is modified. Instead of factorization in the time domain, they assume modification in the spectrum domain, which results in multiplication of $h^{SD}(\tau)$ by a transfer function $h^{CR}(\tau)$. So the relaxation modulus becomes

$$\frac{G_{PL}(t)}{G^0_{N,PL}} = \int_0^\infty \frac{h^{SD}(\tau)h^{CR}(\tau)}{\tau}\exp\left(-\frac{t}{\tau}\right)d\tau + \frac{1}{4Z_S}\sum_{p=1}^{Z_S}\exp\left(-\frac{p^2 t}{\tau_{R,S}}\right) \tag{25}$$

where $G^0_{N,PL} = \frac{4\rho RT}{5M_e}$ and $\tau_R$ is the Rouse time. The second term represents longitudinal modes[14,26] and $\tau_{R,S}$ is treated as an adjustable parameter. As seen in Figure 10, predictions without longitudinal modes are unsatisfactory.

Recall that CR is a result of SD of imaginary chains entangled with the probe chain, so it has two characteristic time scales related to CLF and reptation. At times longer than the reptation time $G^{CR}$ has the form of a 3D Rouse chain relaxation modulus $(\tau_d/t)^{1/2}$, the scaling dependence is similar to those of Milner et al.[20] and Likhtman and McLeish[14] although the prefactor is different. At times shorter than reptation, the CR spectrum is identical to the one reported in refs 20 and 27. So the transfer function consists of two terms

$$\begin{aligned} h^{CR} &:= h^{CR}_{CLF} + h^{CR}_{rep} \\ h^{CR}_{CLF} &:= 2\left[1 - \left(\frac{256\tau}{9\pi^2 Z^4\tau_e}\right)^{1/4}\right](1 - U(\tau - \tau_d)) \\ h^{CR}_{rep} &:= \left[1 - \left(\frac{256\tau_d}{9\pi^2 Z^4\tau_e}\right)^{1/4}\right]\sqrt{\frac{\tau_d}{\tau}}U(\tau - \tau_d) \end{aligned} \tag{26}$$

For a binary blend, the model assumes the simple mixing rule of

$$\begin{aligned} h^{SD}(\tau) &= w_S h^{SD}_S(\tau) + w_L h^{SD}_L(\tau) \\ h^{CR}(\tau) &= w_S h^{CR}_S(\tau) + w_L h^{CR}_L(\tau) \end{aligned} \tag{27}$$

where $w_S$ and $w_L$ are the weight-fractions of the short and the long chains. After substituting eqs 27, 26, and 23 into eq 25, we end up with 16 terms. Several of the terms are 0 due to the different regions in $\tau$ set by unit step and delta functions. Also, for a binary blend of short (S) and long (L) chains, several approximations are made to obtain the expressions from refs 5 and 26.

$$h^{SD}_{rep,S}(\tau)h^{CR}_{CLF,L}(\tau) \to \frac{1}{2}h^{SD}_{rep,S}(\tau)h^{CR}_{CLF,L}(\tau) \tag{28}$$

$$\begin{aligned} h^{SD}_{CLF,L}(\tau)h^{CR}_{CLF,L}(\tau) &\to h^{SD}_{CLF,L}(\tau)h^{CR}_{CLF,L}(\tau)U(\tau_{d,S} - \tau) \\ &+ \frac{\tau}{\tau + \tau_{d,S} - \tau_c}h^{SD}_{CLF,L}(\tau + \tau_{d,S} - \tau_c)h^{CR}_{CLF,L}(\tau + \tau_{d,S} - \tau_c) \\ &\times \frac{U(\tau - \tau_c)U(\tau_c + \tau_{d,L} - \tau_{d,S} - \tau)}{(1 - U(\tau - \tau_{d,L}))^2} \end{aligned} \tag{29}$$

$$\begin{aligned} &h^{SD}_{CLF,L}(\tau)h^{CR}_{rep,S}(\tau) \\ &\to \frac{1}{4}h^{CR}_{CLF,L}(\tau_{d,S})\left(1 + \frac{w_L h^{CR}_{CLF,L}(\tau_{d,S})}{w_S h^{CR}_{CLF,S}(\tau_{d,S})}\right)h^{CR}_{rep,S}(\tau)U(\tau_c - \tau) \end{aligned} \tag{30}$$

$$h^{SD}_{rep,L}(\tau)h^{CR}_{rep,S}(\tau) \to 0 \tag{31}$$

where $\tau_t = \tau_{d,L}$ for SG < 0.064, $\tau_t = w_L\tau_{d,L}$ for SG > 0.064, and $\tau_{d,S}$ and $\tau_{d,L}$ are reptation times of the short and long chains, respectively. Approximation 29 is made in ref 5 but not in ref 26. The full expression for bidisperse $G(t)$ is reported in the Appendix. Note that it is not clear how to apply the PL tube model to systems more disperse than binary.

### Bidisperse LVE Comparisons with Data

Previous work showed good agreement of the DSM LVE predictions with data for monodisperse polymers.[4] Without any additional assumptions or physics, we apply the DSM model to predict bidisperse blends. The model parameters, $\beta$ and $\tau_K$, are fitted to experimental LVE monodisperse data and used to predict other monodisperse and bidisperse LVE measurements.

As pointed out before, there is some experimental inconsistency in the data between different laboratories[4,14] from temperature control, residual solvent, polymer tacticity, thermal degradation, instrument compliance at high frequencies, and sample radius variations. These variations lead to differences in estimations of the $\tau_K$ parameter. Therefore, to predict bidisperse data using $\tau_K$ fitted from monodisperse comparison, both monodisperse and bidisperse data should be taken in the same lab. The data used in our study are reported in Tables 1 and 2.

Figures 1 and 2 show the DSM predictions for monodisperse and bidisperse polymers compared with experimental PS data. For all PS predictions in this work we use $\beta = 15.1$, which corresponds to a plateau modulus value of approximately 250 kPa. DSM predictions are in good agreement with the experimental LVE data assuming only binary entanglements and using a single $\tau_K$ value in each data set. The small deviation of the prediction for PS670 might be the result of polydispersity in experimental data.[4] The disagreement at high frequencies arise from the level of description used in the theory: such short time scales are not present in the DSM model.

In Figure 3, DSM predicts the correct shape for the bidisperse PS LVE, but does not match the data using $\tau_K$ fitted for the

**Table 1. Experimental Data Characteristics and Parameter Fits of Monodisperse Melts**

| code | $10^{-3}M_w$ | $M_w/M_n$ | $T$ (°C) | $N_K$ | $\tau_K$ (ms) | source |
|---|---|---|---|---|---|---|
| PS39 | 39 | 1.07 | 143 | 54 | 6 | 8 |
| PS60 | 60 | 1.04 | 170 | 83 | 0.09 | 11 |
| PS102 | 102 | 1.02 | 130 | 140 | 36 | 12 |
| PS160 | 160 | N/A | 160 | 220 | 0.16 | 7 |
| PS177 | 177 | 1.03 | 170 | 244 | 0.09 | 11 |
| PS355 | 355 | 1.02 | 170 | 489 | 0.045 | 3 |
| PS390 | 390 | 1.06 | 130 | 537 | 36 | 12 |
| PS427 | 427 | 1.05 | 143 | 588 | 6 | 8 |
| PS670 | 670 | N/A | 160 | 922 | 0.16 | 7 |
| PBD22 | 22.8 | 1.05 | 25 | 100 | $0.28 \times 10^{-3}$ | 6 |

**Table 2. Experimental Data Characteristics and Parameter Fits of Bidisperse Melts**

| code | $10^{-3}M_w^{low}$ | $10^{-3}M_w^{high}$ | $T$ (°C) | $w_{low}$ | $\tau_K$ (ms) | source |
|---|---|---|---|---|---|---|
| PS39&427 | 39 | 427 | 143 | 0.8 | 6 | 8 |
| PS60&177%40 | 60 | 177 | 170 | 0.4 | 0.09 | 11 |
| PS60&177%60 | 60 | 177 | 170 | 0.6 | 0.09 | 11 |
| PS102&390 | 102 | 390 | 130 | 0.86 | 16 | 12 |
| PS160&670 | 160 | 670 | 160 | 0.5 | 0.16 | 7 |
| PS191&670 | 191 | 670 | 170 | 0.35 | 0.045 | 3 |
| PBD22&1240 | 22.8 | 1240 | 25 | 0.1 | $0.07 \times 10^{-3}$ | 6 |

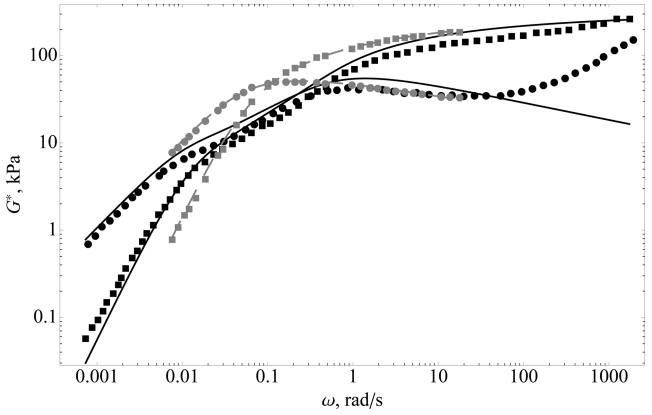


**Figure 1.** Comparison of the DSM LVE predictions with experimental data by Ruybeke et al. Gray symbols are experimental data for PS390 and black symbols are bidisperse mixture PS191&670.[3] Lines are the DSM predictions.

monodisperse systems. Note the crossover of the bidisperse data shifted toward higher frequencies compared to the crossover of the low-molecular-weight monodisperse component. Such a shift contradicts any existing model and most other experimental observations. We suspect that this shift is related to residual solvent in the system. The presence of solvent will result in a decrease in the time scales of the system.

In previous work, we showed a disagreement in the DSM LVE predictions with low-molecular-weight chains that have less than five entanglements. The DSM predicted the correct shape of the low-molecular-weight experimental LVE data; however, the $\tau_K$ value was significantly lower than the value from the high-molecular-weight comparison.[4] The disagreements for low-molecular-weights can be seen in Figures 4 and 5. As mentioned in previous work, the source of the discrepancy is unclear. Similar deviations of the DSM predictions from bidisperse LVE data are observed at the high frequencies before glassy modes take over. This fact suggests that the disagreement is a result of the model coarse-graining. The model assumes that entanglement dynamics is the main determinant of dynamics in polymer melts, which is expected to break down for lightly entangled chains. Also, the model assumes that polymer density and entanglement density

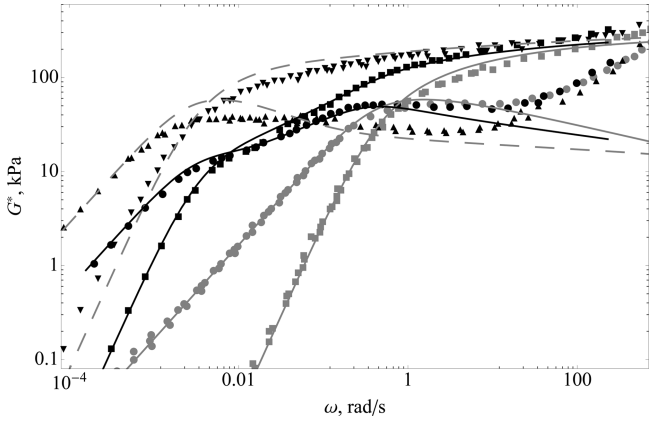


**Figure 2.** Comparison of the DSM LVE predictions with experimental data by Montfort et al. Gray symbols are experimental data for PS160, black triangles are data for PS670, and black squares and circles are bidisperse mixture PS160&670.[7] Lines are the DSM predictions.

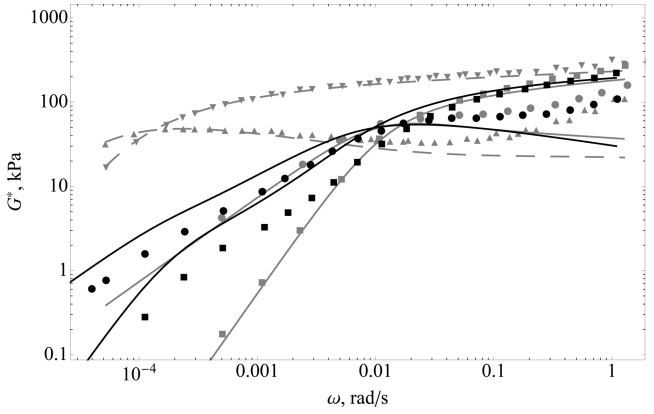


**Figure 3.** Comparison of the DSM LVE predictions with experimental data by Nielsen et al. Gray symbols are experimental data for PS102, black triangles are data for PS390, and black squares and circles are bidisperse mixture PS102&390.[12] Lines are the DSM predictions.

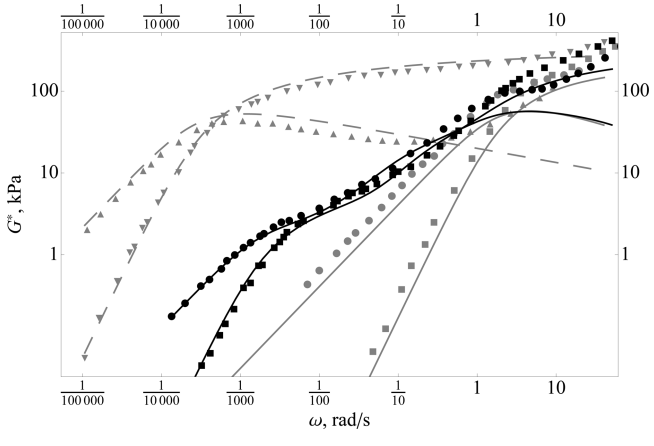


**Figure 4.** Comparison of the DSM LVE predictions with experimental data by Watanabe et al. Gray symbols and black triangles are experimental data for PS39 and PS427 and black squares and circles are bidisperse mixture PS39&427.[8] Lines are the DSM predictions.

are independent of polymer molecular weight, which is incorrect for lightly entangled polymers.[13,29,30] Nevertheless, the LVE prediction by the DSM for the bidisperse systems with lightly entangled chains are satisfactory. The agreement seen in Figures 4 and 5 shows that the model does not require any additional

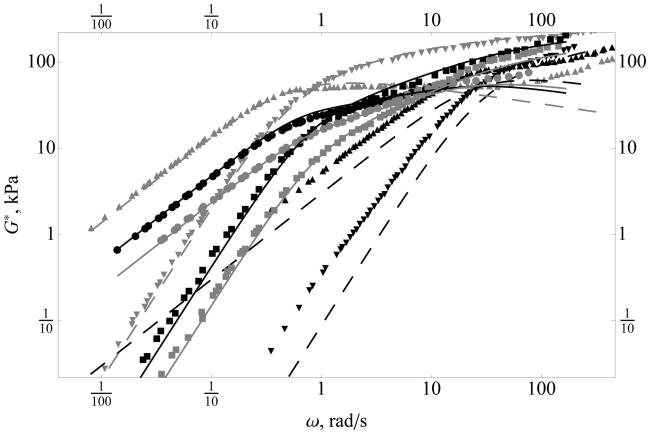


**Figure 5.** Comparison of the DSM LVE predictions (lines) with experimental data by Maier et al. Gray and black triangles are data for PS102 and PS390, black squares and circles are bidisperse mixture PS60&177%40, and gray squares and circles are PS60&177%60.[11].

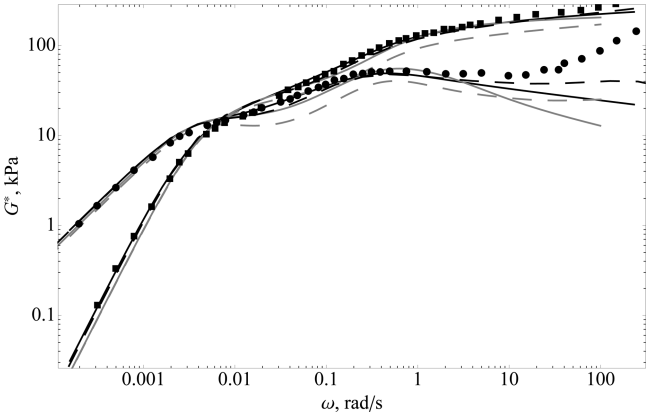


**Figure 6.** Comparison of the tube models and DSM LVE predictions with experimental data for PS160&670 (black symbols).[7] Lines are predictions by the DSM (black solid), TDD-MDR (black dashed), and the PL model (gray solid and dashed).

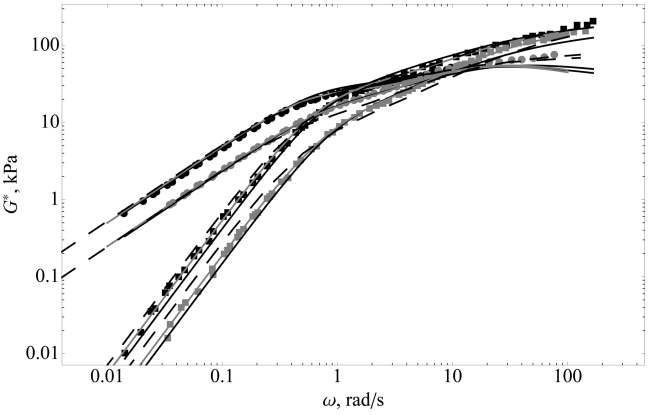


**Figure 7.** Comparison of the tube models and DSM LVE predictions with experimental data for PS60&177%40 (black symbols) and PS60&177%60 (gray symbols).[11] Lines are predictions by the DSM (black solid), TDD-MDR (black dashed), and the PL model (gray).

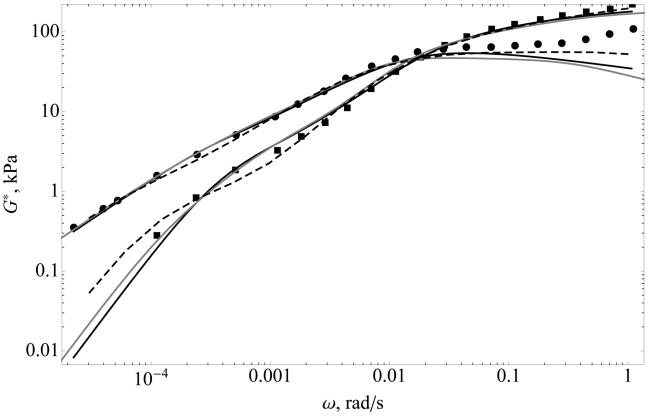


**Figure 8.** Comparison of the tube models and DSM LVE predictions with experimental data for PS102&390 (black symbols).[12] Lines are predictions by the DSM (black solid), TDD-MDR (black dashed), and the PL model (gray).

physics such as tube dilation. It still captures the decrease in the longest relaxation time of the high-molecular-weight chains correctly.

## Comparison of the DSM with Tube Models

We showed above that the DSM agrees with experimental LVE very well. Next we compare tube models with the same bidisperse data, so the time constants for all models will be fitted on bidisperse LVE instead of monodisperse. As seen in Figure 6, Figure 7 and Figure 9 the TDD-MDR and the PL tube model predictions agree with data as well as the DSM for PS160&670, PS60&177%40, PS60&177%60 and PS191&670 blends. The parameters used in these figures are $G_N^0 = 270$ kPa, $K_r = 2.5 \times 10^{-6}$ s/KDa$^3$ and $K_r = 5 \times 10^{-6}$ s/KDa$^2$($\tau_{R,S} = 0.13$ s) for the TDD-MDR model, $\tau_e = 2$ ms and $\tau_{R,S} = 50$ s for the PL model (graysolid line), and $\tau_e = 2$ ms and $\tau_{R,S} = 0.13$ s for the PL model (gray dashed line) in Figure 6; $G_N^0 = 320$ kPa, $K_r = 1.4 \times 10^{-6}$ s/KDa$^3$, and $K_R = 1.4 \times 10^{-6}$ s/kDa$^2$($\tau_{R,S} = 5$ ms) for the TDD-MDR model, and $\tau_e = 1.5$ ms and $\tau_{R,S} = 0.15$ s for the PL model in Figure 7; $G_N^0 = 220$ kPa, $K_r = 0.8 \times 10^{-6}$ s/KDa$^2$, and $K_R = 0.8 \times 10^{-6}$ s/kDa$^3$($\tau_{R,S} = 30$ ms) for the TDD-MDR model, and $\tau_e = 0.65$ ms and $\tau_{R,S} = 0.13$s for the PL model in Figure 9; $G_N^0 = 230$ kPa, $K_r = 0.65 \times 10^{-3}$ *rms*/kDa$^3$, and $K_R = 2 \times 10^{-3}$ s/kDa$^2$-($\tau_{R,S} = 20$ s) for the TDD-MDR model, and $\tau_e = 0.35$ s and $\tau_{R,S} = 100$ s for the PL model in Figure 8. Although, notice that the PL model parameter $\tau_{R,S}$ is always higher than the one used by the TDD-MDR model, especially for PS160&670 blend. In Figure 6 we also show the PL model prediction with $\tau_{R,S}$ consistent with TDD-MDR model; however, the prediction is unsatisfactory. For the PS102&390 blend with SG = 0.074, the TDD-MDR tube model overestimates the longest relaxation time ($\tau_1 = 40000$ s) compared to the DSM ($\tau_1 = 3000$ s), the PL model ($\tau_1 = 1000$ s), and the data, Figure 8. Also, the PL model predicts the wrong position for the crossover point for the PS191&670 blend ($\omega_{x,PL} \approx 0.03$ rad/s, $\omega_{x,exp} \approx 0.1-0.2$ rad/s), as seen in Figure 9. For this blend, SG = 0.019 is lower than the critical value. On the other hand, the TDD-MDR tube model correctly captures the crossover position ($\omega_{x,TDD\text{-}MDR} \approx 0.15$ rad/s) and so does the DSM ($\omega_{x,TDD\text{-}MDR} \approx 0.1$ rad/s). Moreover, the prediction by the TDD-MDR tube model for PS39&427 blend with SG = 1.4 is significantly worse than those by the PL and DSM models, as shown in Figure 10. The fitting parameters for the predictions are $G_N^0 = 320$ kPa, $K_r = 1.5 \times 10^{-5}$ s/kDa$^3$, and $K_R = 1 \times 10^{-3}$ s/kDa$^2$($\tau_{R,S} = 1.5$s) for the TDD-MDR model, and $\tau_e = 0.03$ s and $\tau_{R,S} = 6$ s for the PL model. Moreover, both tube model predictions without longitudinal modes are unsatisfactory for the PS39&427 blend, Figure 10.

## Assumption of Nonbinary Entanglements

We showed that DSM with only binary entanglements predicts the LVE of monodisperse and bidisperse systems well. The model

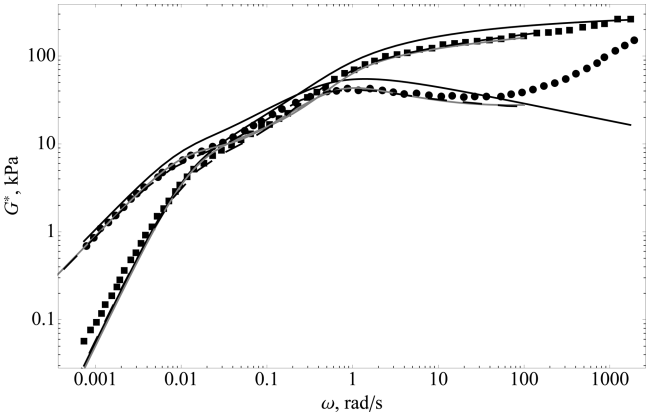


**Figure 9.** Comparison of the tube models and DSM LVE predictions with experimental data for PS191&670 (black symbols).[3] Lines are predictions by the DSM (black solid), TDD-MDR (black dashed), and the PL model (gray).

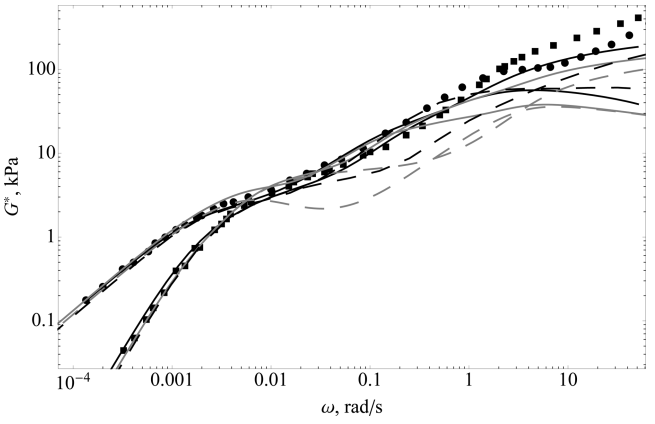


**Figure 10.** Comparison of the tube models and DSM LVE predictions with experimental data for PS39&427 (black symbols).[8] Lines are predictions by the DSM (black solid), TDD-MDR (gray), and the PL model (gray).

does not require any additional physics such as tube dilation and it captures the decrease in the longest relaxation time from its high-molecular-weight monodisperse component properly.

Previously, Nair and Schieber[24] showed that the continuous slip-link model with Rouse-like CR predicts binary blend data better with entanglements that are formed by 5.4 chains on average. However, in ref 4 it has been shown that Rouse-like CR predicts long-time relaxation slower than CD, so the conclusions in ref 24 are model specific and do not apply to the DSM with CD. Therefore, we test the assumption of binary entanglements. Higher-order entanglements require more than two chains per entanglement. If one of the chains abandons an entanglement, the entanglement is destroyed for all of the chains.

We compare LVE predictions for the PS102&390 bidisperse blend with SG = 0.074, assuming binary and ternary entanglements. As seen in Figure 11, the longest relaxation time for the blend is significantly shorter for the DSM with ternary entanglements than observed experimentally and predicted by DSM with binary entanglements. If we assume higher entanglement complexity, the deviation will increase. This result suggests that the assumption of binary entanglements is better than higher-order ones for DSM.

## Experiments of Liu et al.

Liu et al.[6] tried to probe the chain relaxation modulus in a fixed environment experimentally. They measured the dynamic

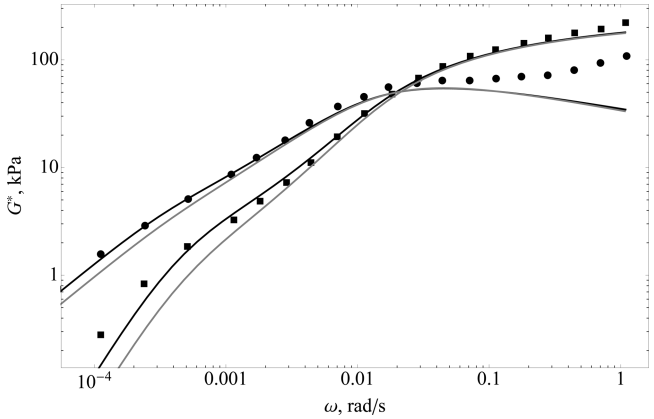


**Figure 11.** Comparison of the DSM LVE predictions assuming binary (black lines) and ternary (gray lines) entanglements with PS102&390 experimental data (black symbols).[12].

modulus of 10% by mass probe chains in a very-high-molecular-weight matrix. The measurements clearly show two distinct peaks of $G''$ at low and high frequencies. They naturally assumed that in the blend the high-molecular-weight matrix relaxation has a much slower time-scale than relaxation of the low-molecular-weight probe chains. Therefore, the position of the low-frequency peak is determined by relaxation of the diluted high-molecular-weight matrix only, and the position of the high-frequency peak, $G''_{peak}$, is determined by relaxation of the probe chains in a nearly fixed environment. As a result, they concluded that LVE of the blend minus LVE of the diluted matrix is proportional to LVE of the probe chains in a fixed environment. From several LVE measurements of blends with different probe-chain molecular-weights they showed that the $G''_{peak}$ corresponding frequency, $\omega_{peak}$, scales with molecular-weight of the probe chains as $M_w^{-3.1}$. They also calculated a retardation factor $\omega_{mono}/\omega_{peak}$, where $\omega_{mono}$ is the frequency at $G''_{peak}$ for monodisperse probe chains. The retardation factor was significantly higher (above 3)[22] than tube models (below 2.5)[22] or DSM (~3)[4] predictions. Liu et al. concluded that relaxation of the environment affects chain relaxation more than existing models predict. They also concluded that the observed zero-shear-rate viscosity scaling of 3.5 is a result of environment relaxation and not CLF. As a result, they suggested that the contribution to relaxation from CLF is overestimated in tube models.

In contrast to tube models, the DSM model does not specify contributions to chain relaxation from reptation or longitudinal modes—it arises from the model. DSM also predicts that CD does not affect zero-shear-rate viscosity scaling with molecular weight,[4] which contradicts Liu et al. In previous work, we suggested that the disagreement might result from CD relaxation of the matrix due to SD of the probe chains in Liu's experiments.[4]

In fact, the factorization assumption predicts that the normalized relaxation modulus, $\bar{G}_B(t) = G_B(t)/G_N^0$, of the bidisperse blend is

$$\bar{G}_B(t) = (w_L\bar{G}_L^{SD}(t) + w_S\bar{G}_S^{SD}(t))(w_L\bar{G}_L^{CD}(t) + w_S\bar{G}_S^{CD}(t)) \quad (32)$$

where $\bar{G}_L^{SD/CD}$ is the normalized stress relaxation due to long chain dynamics only and $\bar{G}_S^{SD/CD}$ is the normalized stress relaxation due to short chain dynamics. The weight fraction of the probe chains is much smaller than weight fraction of the matrix, so we neglect terms of $w_S^2$. Also, for $t \ll \tau_{d,L}$, the stress relaxation by the matrix dynamics can be neglected

compared to the stress relaxation by the probe dynamics; in other words, $\bar{G}_S^{SD/CD}\bar{G}_L^{SD/CD} \sim \bar{G}_S^{SD/CD}$. Then it is straightforward to show that $\bar{G}_B(t)$ without the matrix contribution, the quantity Liu et al. plotted in their Figure 3b, becomes

$$\bar{G}_B(t) - w_L^2\bar{G}_L(t) \simeq w_S(\bar{G}_S^{SD}(t) + \bar{G}_S^{CD}(t)) \qquad (33)$$

Note that the relative contribution is independent of the matrix molecular-weight or weight-fraction as long as the matrix relaxation is much slower than the relaxation of the probe chains. In other words, LVE measurements of a probe chain in a high-molecular-weight matrix are not measuring stress relaxation by SD only, but an average of relaxations by SD and CD, because probe chains remove constraints that they impose on the environment.

Liu et al. neglected the second term on the right side of eq 33 in their analysis. Although, they misinterpreted the results, their experiments have significant value. As we have shown in previous work, the DSM individual SD and CD relaxation processes are very different from SD and CD in the Likhtman and McLeish tube model.[4] However, monodisperse LVE measurements observe the product of the two relaxation processes, and this product is very similar for DSM and the Likhtman and McLeish tube model.[4] Thus, monodisperse experiments could not differentiate between the two models. As we can see, probe rheology measures the average of the two processes (within the factorization assumption), which is different for the DSM and the Likhtman and McLeish tube model. Although the Likhtman and McLeish tube model is derived for monodisperse systems, it is possible to generalize their model to apply to bidisperse blends. However, the generalization is outside of the scope of this paper; therefore, we will avoid the comparison here.

In this work we included contribution from the matrix relaxation due to CD induced by the probe chains. We have fitted $\beta$ and $\tau_K$ to the monodisperse PBD 22 kDa LVE experimental data, and the fit (gray continuous line) and the data (■) are plotted in Figure 12. Note that LVE data of PBD22 is shifted vertically by a factor of 4 for better visualization. The parameter values for PBD are $\beta = 5.1$, which corresponds to $G_N^0 = 1.7$ MPa and $\tau_K = 0.07\ \mu$s at 25 °C. Note that our $G_N^0$ value is significantly higher than the one reported in ref 6 ($G_N^0 = 1.15$ MPa). Without any adjustments to the $\tau_K$ value, we predict the dynamic modulus of the bidisperse blend. The DSM model allows us to calculate contributions to the blend relaxation from the probe chains and the matrix separately. The relaxation modulus of the matrix shows significant relaxation ($\sim 10\% G_N^0$) on the time scale of the probe chain relaxation. This matrix relaxation was neglected by Liu et al. We also calculated the dynamic modulus of the diluted matrix by setting $\beta_d = 5.7$ ($G_{N,d}^0 = 1.4$ MPa) and subtracted it from the blend LVE prediction. The resulting LVE after subtraction (black line) has a plateau modulus of $G_{N,b-d}^0 = 0.3$ MPa. It is compared to the experimental data (circles) and to the DSM prediction of the probe chain relaxation by SD only (gray dashed) in Figure 12.

As shown in Figure 12, the DSM LVE prediction for the blend minus diluted matrix (black lines) agrees with experimental data very well; however, we performed a vertical shift of the prediction by 0.05 MPa to match the data. The shift forces the plateau modulus to become 0.25 MPa, the value similar to that reported by Liu et al. This 20% vertical shift will not affect $\omega_{peak}$ and the retardation factor. Therefore, the DSM predicts the correct position of $\omega_{peak}$ and the retardation factor for the probe chains. In Figure 12 we also show LVE of the PBD 22 kDa stress relaxation by SD only as predicted by the DSM (gray dashed lines). From the figure it is clear that the

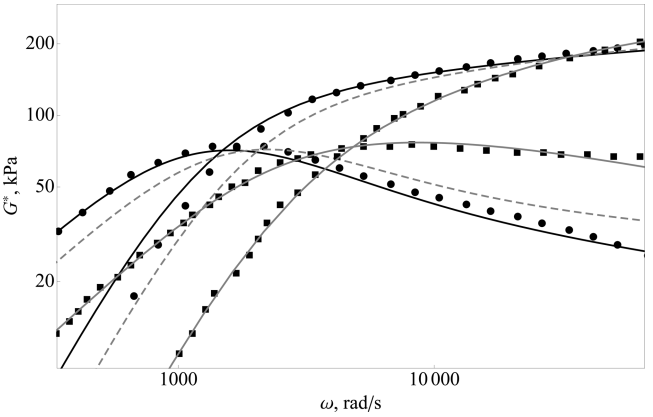


**Figure 12.** Comparison of the DSM predictions with experimental data (symbols) by Liu et al. The circles are LVE data of PBD22&234 with subtracted LVE of diluted PBD 234 kDa (Figure 3 in ref 6). The squares are LVE data of the monodisperse probe chains shifted vertically by a factor of 4 for better visualization. Lines are LVE predictions of the monodisperse probe chain relaxation (gray continuous), probe chain stress relaxation by SD only (gray dashed) and probe chain relaxation including CD from the matrix (black) by the DSM.

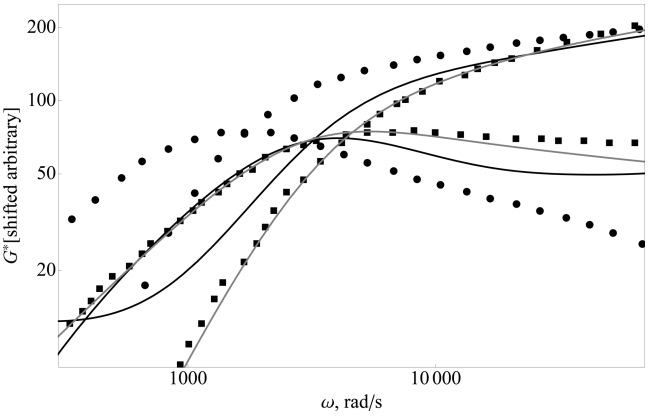


**Figure 13.** Comparison of the PL tube model predictions with experimental data (symbols as in Figure 12) by Liu et al. Lines are LVE predictions by the Park and Larson tube model. The squares are LVE data of the monodisperse probe chains shifted vertically by a factor of 4 for better visualization. Lines are LVE predictions of the monodisperse probe chain relaxation (gray continuous) and probe chain relaxation including CR from the matrix (black) by the Park and Larson tube model.

predicted LVE, which is similar to the average of $\bar{G}_S^{SD}$ and $\bar{G}_S^{CD}$, relaxes slower than $\bar{G}_S^{CD}$ only; in other words, the contribution from the matrix relaxation due to CD from the short chains decreases $\omega_{peak} = 1590$ rad/s compared to the value for the relaxation of short chains by SD, only $\omega_{peak} = 2240$ rad/s, as expected. The results show that DSM predicts Liu et al. experimental data and explains the retardation factor increase but disagrees with their conclusions. The high-molecular-weight matrix CD relaxation is not negligible compared to the probe chain relaxation.

We performed the same procedure to compare LVE predicted by the PL tube models.[26] The model parameters were fitted to the probe monodisperse data ($M_e = 1.57$ kDa and $\tau_e = 0.14\ \mu$s). The monodisperse LVE data and PL model are plotted in Figure 13 as squares and the gray continuous lines. Without any adjustment of the parameters, we use the PL tube model to predict Liu et al. probe rheology data, shown in Figure 13 as black circles and a black line, accordingly. It is clear that the prediction of the probe rheology experiments by the PL tube model is unsatisfactory.

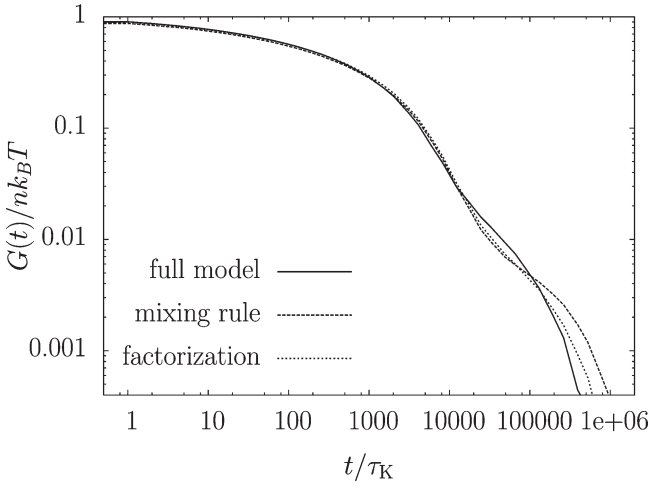


**Figure 14.** Relaxation moduli predicted by DSM. Lines are predictions by the DSM.

### Factorization Assumption

One of the essential assumptions in tube models is factorization, which is necessary given the tube models' typical level of description. It assumes that polymer relaxation is proportional to a product of relaxation by SD only and relaxation by CR only. Therefore, the influence of SD on CR and vice versa are neglected. Although the PL tube model avoids factorization in the time domain, it still requires spectrum factorization. We examined the time factorization assumption with DSM for *monodisperse* polymers and found it to be reasonable.[4] However, it is expected that interactions between SD and CD are stronger in *bidisperse* blends. Therefore, we tested if the factorization assumption can also be applied to bidisperse systems. In addition, we tested the mixing rule (eq 19), which is used by the TDD-MDR model and predicts blend relaxation based solely on relaxation of its monodisperse components. The DSM has a more-detailed level of description, so it does not require factorization or a mixing rule, and we can use DSM to check two assumptions made in tube models.

We have calculated $G^{SD}(t)$ and $G^{CD}(t)$ for the PS102&390 blend using DSM and compared their product, normalized by $G_N^0$, with the DSM $G(t)$ prediction. Note that $G^{SD}(t)$ for the blend is a superposition of $G^{SD}(t)$ of its monodisperse components. The factorized prediction is shown in Figure 14 as "factorization" (dotted line). Clearly, the product of the two relaxation moduli overestimates the longest relaxation time of the blend. So the interaction between SD and CD processes are significant in bidisperse blends. Note, that a similar overestimation of the longest relaxation times was observed in the TDD-MDR and PL tube models prediction of the PS102&390 blend.

We have shown above that in bidisperse blends, SD and CD significantly affect each other. Equally important to know is if CD of the short chains affects CD of the long chains. To analyze the effect, we calculate a superposition of $G^{CD}(t)$ of the monodisperse components multiplied by a superposition of $G^{SD}(t)$. The procedure is similar to the mixing rule, eq 19, where all contributions come from monodisperse predictions. The resulting curve is displayed in Figure 14, labeled as "mixing rule" (dashed line). As shown in the figure, the relaxation modulus predicted by the mixing rule is above that predicted by the factorization assumption. This fact implies that the presence of the short-chain−long-chain entanglements reduces the longest relaxation time of the long-chain CD relaxation modulus.

The above effects are more significant for the blends of very short and very long chains, SG $\gg$ 1. The decrease of the longest relaxation time of the long-chain CD due to the presence of the entanglements with short chains is compensated by the tube dilation process, which instead reduces reptation time, in tube models.

A decrease of the longest relaxation time of the long chains due to the presence of short chains is observed experimentally.[9] However, experiments are unable to determine whether the effect is due to a decrease of the SD-longest-relaxation-time or the CD-longest-relaxation-time. Tube models postulate that the effect is related to a decrease of the SD-longest-relaxation-time and mimic it by the tube dilation process. In the DSM, the effect is not postulated but arises from the model's self-consistency. We observe that the presence of short chains decreases the longest relaxation time of both processes: SD and CD. However, SD dominates over CD, and therefore, the decrease of the CD-longest-relaxation-time is unimportant.

### Conclusions

By comparison with data and less-detailed tube models, the DSM is able to draw several important conclusions. Without any additional physics, we applied DSM to predict bidisperse LVE. Both fitting parameters of the model, $\beta$ and $\tau_K$, were determined from the monodisperse LVE comparison with data. Using these parameters, the DSM with only binary entanglements predicts bidisperse LVE at least as well as the TDD-MDR tube model with 64 adjustable parameters ($K_r$, $K_R$, $M^*$, and $M_e$) and the PL tube model with four parameters ($M_e$, $\tau_e$, $\tau_R$, and SG), including longitudinal modes. The PL model is somewhat more difficult to calculate than the TDD-MDR model, but both are substantially easier than DSM calculations. Even with significant difference in molecular-weight between long and short chains, in which case the PL model requires the SG parameter, the DSM predicts blends LVE without any modifications relative to the monodisperse case. The fundamental and self-consistent implementation of CD avoids any tube dilation process required by CR in tube models.

We showed that only DSM with binary entanglements can predict probe rheology and monodisperse LVE data at the same time. The failure of the tube models is a result of different contributions from SD and CD to the relaxation modulus compare to the DSM.[4]

We tested a factorization assumption and mixing rule for bidisperse systems. We showed that SD and CD can not be treated as independent processes, as typically assumed in tube models. Such an assumption introduces an error, if applied to the DSM, that overestimates the longest relaxation time.

We generalized the DSM to allow entanglements of any complexity. We showed that binary interactions between chains is not only a sufficient, but a required assumption for the DSM. The assumption is also supported by our analysis of Liu et al.'s probe rheology experimental data. So the ad hoc exponent of 2.2 in the MDR theory could not be explained by complex entanglements, but rather might be related to compensation of the error from decoupling SD and CR.

**Acknowledgment.** Support of this work by the National Science Foundation under Grant No. NSF-SCI 05063059 and Army Research Office Grant W911NF-08-2-0058 is gratefully acknowledged. The authors are also grateful for insightful conversations with Prof. David Venerus.

### Park and Larson Tube Model in Spectrum Domain

We have shown above our own interpretation of the PL tube model applied to bidisperse systems. From eqs 19, 23, 25, and 26, $G_{PL}$ consists of 16 terms. After applying approximations 28, 29, 30, 31 we obtain an expression consistent

with the one reported in ref 5 (eq 19), but in the spectrum domain.

$$\frac{G(t)}{G_N^0} = \frac{1}{2}\int_0^{\tau_{d,S}} \frac{1}{\tau}\left\{ w_S\left[1-\left(\frac{256\tau}{9\pi^2 Z_S^4 \tau_e}\right)^{1/4}\right] + w_L\left[1-\left(\frac{256\tau}{9\pi^2 Z_L^4 \tau_e}\right)^{1/4}\right]\right\} \times \left[ w_S\left(\frac{256\tau}{9\pi^2 Z_S^4 \tau_e}\right)^{1/4} + w_L\left(\frac{256\tau}{9\pi^2 Z_L^4 \tau_e}\right)^{1/4}\right] \exp\left(-\frac{t}{\tau}\right) d\tau + \frac{w_L}{2}\left[1-\left(\frac{256\tau_{d,S}}{9\pi^2 Z_L^4 \tau_e}\right)^{1/4}\right] \times \left\{ w_S\left[1-\left(\frac{256\tau_{d,S}}{9\pi^2 Z_S^4 \tau_e}\right)^{1/4}\right] + w_L\left[1-\left(\frac{256\tau_{d,S}}{9\pi^2 Z_L^4 \tau_e}\right)^{1/4}\right]\right\} \int_{\tau_{d,S}}^{\tau_c} \frac{\sqrt{\tau_{d,S}}}{\tau\sqrt{\tau}} \exp\left(-\frac{t}{\tau}\right) d\tau + \frac{w_L^2}{2}\int_{\tau_{d,S}}^{\tau_t} \left[1-\left(\frac{256\tau}{9\pi^2 Z_L^4 \tau_e}\right)^{1/4}\right]\left(\frac{256\tau}{9\pi^2 Z_S^4 \tau_e}\right)^{1/4} \exp\left(-\frac{t}{\tau+\tau_c-\tau_{d,S}}\right)\frac{d\tau}{\tau} + w_S\left[1-\left(\frac{256\tau_{d,S}}{9\pi^2 Z_S^4 \tau_e}\right)^{1/4}\right]\left\{ w_S\left[1-\left(\frac{256\tau_{d,S}}{9\pi^2 Z_S^4 \tau_e}\right)^{1/4}\right] + w_L\left[1-\left(\frac{256\tau_{d,S}}{9\pi^2 Z_L^4 \tau_e}\right)^{1/4}\right]\right\} \frac{8}{\pi^2} \times \sum_{p\text{odd}} \frac{1}{p^2} \exp\left(-\frac{p^2 t}{\tau_{d,S}}\right) + w_L^2\left[1-\left(\frac{256\tau_t}{9\pi^2 Z_L^4 \tau_e}\right)^{1/4}\right]^2 \frac{8}{\pi^2}\sum_{p\text{odd}} \frac{1}{p^2} \exp\left(-\frac{p^2 t}{\tau_t}\right) \quad (34)$$

## References and Notes


(1) Marrucci, G. *J. Polym. Sci., Polym. Phys. Ed.* **1985**, *23*, 159–177.
(2) Rubinstein, M.; Helfand, E.; Pearson, D. S. *Macromolecules* **1987**, *20*, 822–829.
(3) van Ruymbeke, E.; Keunings, R.; Stephenne, V.; Hagenaars, A.; Bailly, C. *Macromolecules* **2002**, *35*, 2689–2699.
(4) Khaliullin, R. N.; Schieber, J. D. *Macromolecules* **2009**, *42*, 7504–7517.
(5) Park, S. J.; Larson, R. G. *Macromolecules* **2004**, *37*, 597–604.
(6) Liu, C.-Y.; Halasa, A. F.; Keunings, R.; Bailly, C. *Macromolecules* **2006**, *39*, 7415–7424.
(7) Montfort, J. P.; Marin, G.; Arman, J.; Monge, P. *Rheol. Acta* **1979**, *18*, 623–628.
(8) Watanabe, H.; Kotaka, T. *Macromolecules* **1984**, *17*, 2316–2325.
(9) Watanabe, H.; Ishida, S.; Matsumiya, Y.; Inoue, T. *Macromolecules* **2004**, *37*, 6619–6631.
(10) Rubinstein, M.; Colby, R. H. *J. Chem. Phys.* **1988**, *89*, 5291–5306.
(11) Maier, D.; Eckstein, A.; Friedrich, C.; Honerkamp, J. *J. Rheol.* **1998**, *42*, 1153–1173.
(12) Nielsen, J. K.; Rasmussen, H. K.; Hassager, O.; McKinley, G. H. *J. Rheol.* **2006**, *50*, 453–476.
(13) Foteinopoulou, K.; Karayiannis, N. C.; Mavrantzas, V. G.; Kröger, M. *Macromolecules* **2006**, *39*, 4207–4216.
(14) Likhtman, A. E.; McLeish, T. C. B. *Macromolecules* **2002**, *35*, 6332–6343.
(15) des Cloizeaux, J. *Europhys. Lett.* **1988**, 437.
(16) Khaliullin, R. N.; Schieber, J. D. *Phys. Rev. Lett.* **2008**, *100*, 188302.
(17) Schieber, J. D.; Neergaard, J.; Gupta, S. *J. Rheol.* **2003**, *47*, 213–233.
(18) Pattamaprom, C.; Larson, R. G.; Van Dyke, T. J. *Rheol. Acta* **2000**, *39*, 517–531.
(19) Graessley, W. *Adv. Polym. Sci.* **1982**, 67–117.
(20) Milner, S. T.; McLeish, T. C. B.; Young, R. N.; Hakiki, A.; Johnson, J. M. *Macromolecules* **1998**, *31*, 9345–9353.
(21) Struglinski, M. J.; Graessley, W. W. *Macromolecules* **1985**, *18*, 2630–2643.
(22) Liu; He; Keunings, R.; Bailly, C. *Macromolecules* **2006**, *39*, 3093–3097.
(23) Doi, M.; Takimoto, J.-I. *Proc. R. Soc. London, Ser. A* **2003**, *361*, 641–652.
(24) Nair, D. M.; Schieber, J. D. *Macromolecules* **2006**, *39*, 3386–3397.
(25) Baumgaertel, M.; Schausberger, A.; Winter, H. H. *Rheol. Acta* **1990**, *29*, 400–408.
(26) Park, S. J.; Larson, R. G. *J. Rheol.* **2006**, *50*, 21–39.
(27) Milner, S. T.; McLeish, T. C. B. *Phys. Rev. Lett.* **1998**, *81*, 725.
(28) *Handbook of Mathematical Functions with Formulas, Graphs, and Mathematical Tables*, 9th printing; Abramowitz, M., Stegun, I. A., Eds.; Dover: New York, 1972.
(29) Mavrantzas, V. G.; Boone, T. D.; Zervopoulou, E.; Theodorou, D. N. *Macromolecules* **1999**, *32*, 5072–5096.
(30) Tzoumanekas, C.; Lahmar, F.; Rousseau, B.; Theodorou, D. N. *Macromolecules* **2009**, *42* (19), 7485–7494.
(31) van Ruymbeke, E.; Keunings, R.; Bailly, C. *J. Non-Newtonian Fluid Mech.* **2005**, *128*, 7–22.